Arabian Journal of Chemistry (2022) **15**, 103588

King Saud University

Arabian Journal of Chemistry

www.ksu.edu.sa
www.sciencedirect.com

ORIGINAL ARTICLE

CaO nanoparticles incorporated metal organic framework (NH_2-MIL-101) for Knoevenagel condensation reaction

Huda I. Aljaddua, Mosaed S. Alhumaimess, Hassan M.A. Hassan *

Department of Chemistry, College of Science, Jouf University, PO Box 2014, Sakaka, Saudi Arabia

Received 20 September 2021; accepted 21 November 2021
Available online 25 November 2021

KEYWORDS

Metal-organic frameworks;
Eggshell;
MOFs;
CaO;
Knoevenagel reaction;
Heterogeneous catalysis

Abstract Porous materials based on NH_2-MIL-101(Cr) MOF and their hierarchical acid-base composite with non-precious CaO was successfully prepared using a one-pot scalable hydrothermal approach. The composites were characterized by XRD, FTIR, UV–vis, ^{1}HNMR, TGA, N_2 adsorption–desorption isotherms, HRTEM and FESEM. The quantitative assessment of the basic sites was performed by benzoic acid titration. The results reveal that there is no remarkable structural alterations in the NH_2-MIL-101(Cr) after incorporation of CaO. Raising the CaO content boosted the strength of and content of Lewis basic sites from 0.31 to 1.34 mmol g^{-1} due to the incorporation with CaO (0.04). Knoevenagel condensation reactions were performed as the probe reactions over the CaO/NH_2-MIL-101(Cr) catalysts. Both basic and acidic sites potentially boosted the reaction. Pure NH_2-MIL-101(Cr) display the catalytic conversion in the reaction (11%) which could be attributed weak basic sites on the NH_2-MIL-101(Cr) framework. However, the conversion (%) was potentially increased over NH_2-MIL-101(Cr) loaded with various content of CaO. The highest performance of (99%) conversion was achieved for (0.04) CaO/NH_2-MIL-101(Cr) catalyst. Exceptional conversion above 90% have been obtained for benzaldehyde derivatives both withdrawing and donating electron moieties. The composites can be recycled in four runs with a very small loss in performance. Furthermore, the composites produced tend to be feasible for various catalytic processes, exploring new avenues to produce of novel inorganic and organic composite materials as heterogeneous catalysts.

1. Introduction

Recently, the production of heterogeneous catalysts play an important role in industrial processes (Cui et al., 2018; Matsunaga and Shibasaki, 2013; Matsunaga and Shibasaki, 2014). Solid bases, a form of heterogeneous catalyst, have gotten a lot of attention recently because they have a number of advantages over their liquid counterparts, including reliability and reusability. After the reaction in a heterogeneous cata-

* Corresponding author.
E-mail address: hmahmed@ju.edu.sa (H.M.A. Hassan).
Peer review under responsibility of King Saud University.

Production and hosting by Elsevier

https://doi.org/10.1016/j.arabjc.2021.103588
1878-5352

lyst was completed, the catalyst could be separated very simply, making it practical to use several times. As a result, it offers a cost-effective and eco-friendly way to fabricate chemicals, which is ideal for green-chemistry and long-term growth (Zhu et al., 2017). The main focus of heterogeneous catalysis work is on developing materials with desirable architectures and examining the structure–activity correlation between catalysts and reactions. Also, the impact of defects on catalytic performance is receiving more attention, and controlling defects in catalytic materials has emerged as a key route in the development of catalyst microstructures (Xie et al., 2020). Metal-organic frameworks (MOFs), a versatile porous compound, are an instance of solid heterogeneous catalysts; they are a new class of microporous components with enhanced versatility, large surface areas, and porosity. Possibilities for modification of MOFs with comparable catalytic active sites, enabling for catalysis by a variety of functional moieties as well as bifunctional catalysis (Yang and Gates, 2019; Wang et al., 2020; Cheng et al., 2020; Tran et al., 2011; Abd El Rahman et al., 2014; Hassan et al., 2017; El-Shall et al., 2009; Alhumaimess et al., 2020). Of different MOFs, chromium (Cr)-based MOFs are the easiest to prepare and have a greater surface area, porosity, very large pore volume, chemical and thermal stability, excellent moisture stability, and plenty of unsaturated active chromium sites. Also, it exhibits two kind of mesoporous diameters 2.9 and 3.4 nm, respectively, which are available through two microporous cavities of 1.2 and 1.6 nm (Abd El Rahman et al., 2014; Hassan et al., 2017; El-Shall et al., 2009; Alhumaimess et al., 2020). Integration of metal cations and functional moieties on organic ligand could further expand the synergies in MOFs. MOFs containing both Lewis acidic and basic sites concurrently is a committed catalyst for the frustrating solid acid-base catalyst. There is an unlimited ability to modify the pores within MOFs, where several of guest molecules can be found. For enhancing catalysis, some of functional molecules are combined with MOFs, like metal oxides. The enhanced catalysis is depend on the synergistic phenomenon of a coupling of various features of MOFs and these molecular guests. The design of metal oxide (MO)/MOFs composites affords an efficient hybrid catalysis role. It is possible to effectively restrict the use of the periodic cavities of MOFs, to limit the aggregations of MO nanoparticles, lead to consistent and stable nano-structures and facilitated diffusion and transport (Wee et al., 2014; Liu et al., 2013; Zhang et al., 2013; Wang et al., 2011; Li et al., 2020). One of the most widely implemented organic transformations involve the C—C coupling of aldehydes with substances having the activated methylene ring (Li et al., 2018). This incredibly valuable chemical synthesis process that is catalyzed by soluble basic catalysts. However, usage of homogeneous catalyst attendant problems in catalyst recovery and reuse. Therefore, several powerful and reusable solid-base catalyst were utilized for the Knoevenagel reaction, such as functionalized MCM-41 (Parida and Rath, 2009), ionic liquids (Zhao et al., 2013); carbon-based materials (Villa et al., 2010) and, other amine-tagged supports (Mondal et al., 2011). The use of aromatic carboxylic acids as linkers that have an amino moiety could contribute to the development of amino-tagged MOFs (Aromi, 2011 ; Hasegawa et al., 2007). Nevertheless, due to the lower pKa and electron densities triggered by the carboxylate groups, amine-tagged MOFs suffering from lower condensation reactivity. This could be attributed to the aromatic amino group's electron density was pushed away by two neighboring electron-withdrawing carboxylate groups, which contributed in lower the condensation performance (Stewart and Dolman, 1967). Furthermore, due to nitrogen's productive coordination with metal ions, nitrogen-rich MOFs may be suffering from weak basicity (Zhang et al., 2012). On the other hand, amine anchoring using homogeneous amine substances on metal centers of MOFs has been investigated as an opportunity to access catalysts for condensation reactions (Hwang et al., 2008; Li et al., 2012). Base leaching and poor catalyst recycling, on the other hand, could be expected, as has been demonstrated in some cases (Chen et al., 2014). Despite considerable progress in MOF boosted Knoevenagel process (Trilla et al., 2009), facile approaches for obtaining potentially powerful heterogeneous basic MOF catalysts are lacking.

In this work, a series of basic MOF composite catalysts comprising alkaline-earth-metal oxide like CaO stemming from eggshell as solid waste were fabricated by in-situ growing hydrothermal approach.

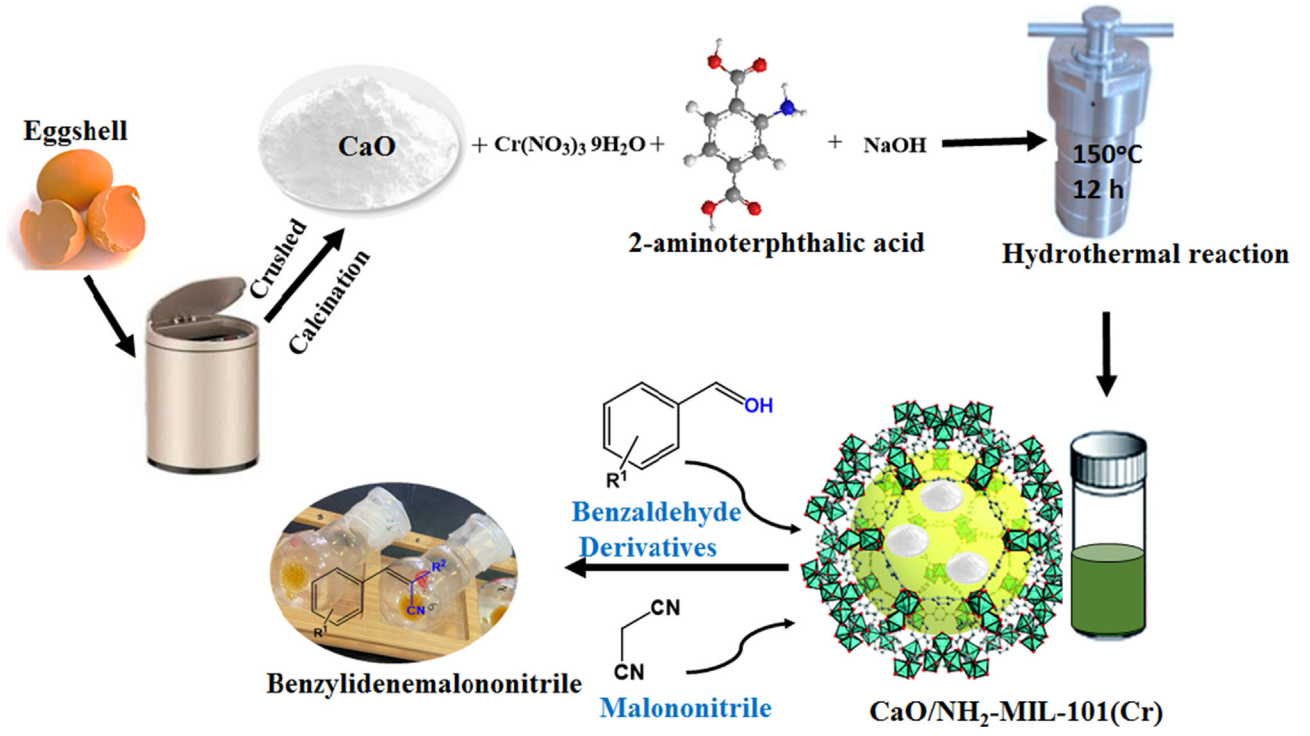

Fig. 1 Schematic representation displaying the synthesis the fashioned composite CaO/NH_2-MIL-101.

The in-situ growing approach has been provided to avoid leaching of the guest species. The composite nanoparticles comprising amine-tagged MIL-101(Cr) with both Lewis acidic and basic sites and CaO afford strong Lewis basic sites, rendering CaO/NH_2-MIL-101 (Cr) composite robust and durable catalyst for Knoevenagel condensation.

2. Experimental

2.1. Materials

Malononitrile (≥99%), 4-nitrobenzaldehyde (98%), 4-bromobenzaldehyde (99%), 4-chlorobenzaldehyde (97%), P-anisaldehyde (98%), P-tolualdehyde (97%), Methyl cyanoacetate (99%), 3-bromobenzaldehyde (97%), Chromium (III) nitrate nonhydrate ($Cr(NO_3)_3{\cdot}9H_2O$, 99%), Tetrahydofuran (THF, ≥ 99.9%), Sodium hydroxide (NaOH, ≥ 98%). Benzaldehyde (≥99%) were procured from Sigma-Aldrich Co., USA. 4-Cyano-benzaldehyde (98%) was obtained from Merck KGaA Co., Germany. Aminoterphthalic acid (H_2N-BDC, 99%) was provided by Acros Organics. Toluene (99.9%) was gotten by Scharlau. Benzoic acid (99.5%) was obtained from Beijing Chemical Works. All materials utilized as procured without any further treatment. Eggshells waste used to synthesize CaO. Distilled water applied in all the experiments was obtained by Milli-Q direct 8 purification system (Millipore, France).

Table 1 NH_2-MIL-101(Cr) and CaO dosage for the preparation of composite catalysts.

Mass Ratio	$Cr(NO_3)_3{\cdot}9H_2O$	H_2N-H_2BDC	CaO	Ca content[a]
NH_2-MIL-101(Cr)/CaO = 27.19	0.400 g	0.180 g	0.010 g	0.006
NH_2-MIL-101(Cr)/CaO = 13.59	0.400 g	0.180 g	0.020 g	0.0132
NH_2-MIL-101(Cr)/CaO = 9.06	0.400 g	0.180 g	0.030 g	0.0199
NH_2-MIL-101(Cr)/CaO = 6.79	0.400 g	0.180 g	0.040 g	0.0262

[a] Determined by ICP-OES.

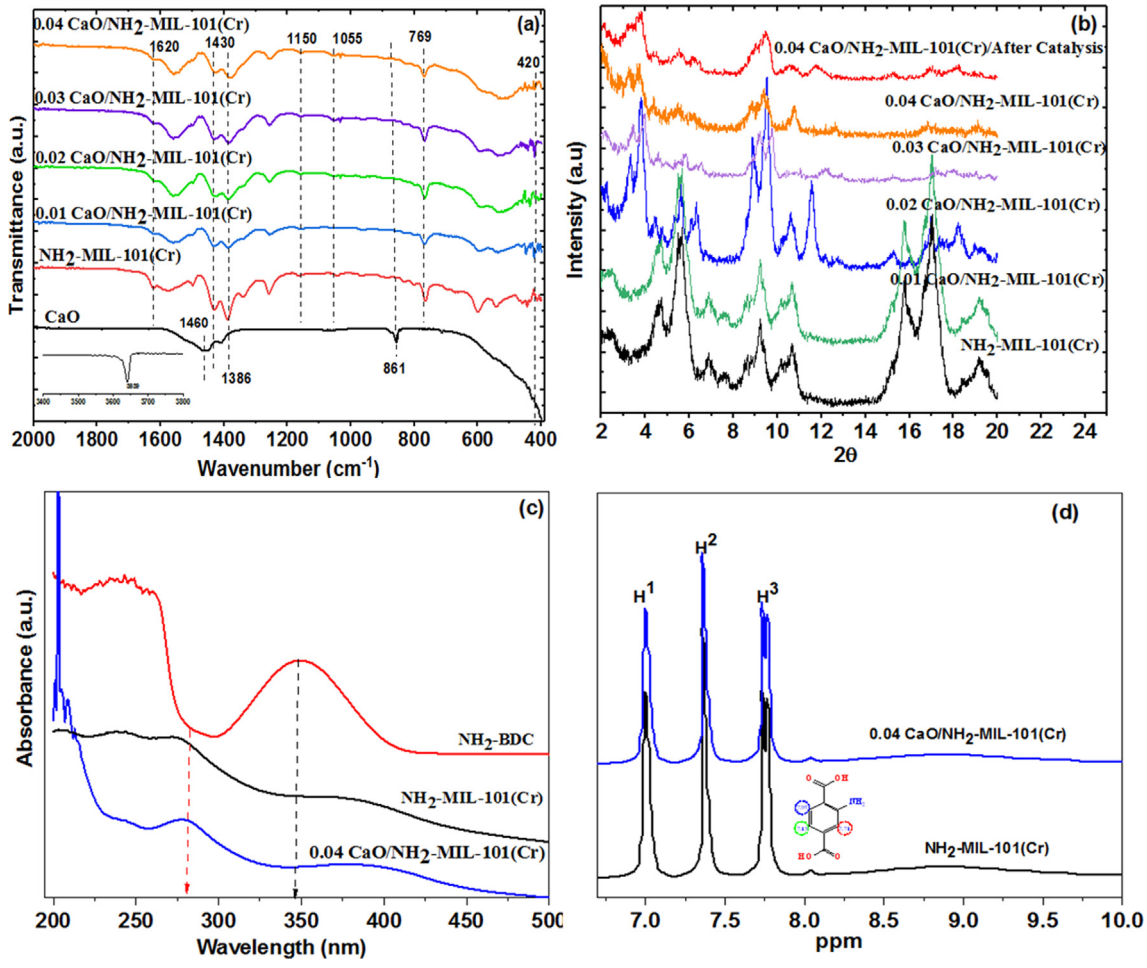

Fig. 2 (a) FT-IR spectra, (b) XRD patterns, (c) UV–vis, and (d) ^{1}HNMR spectra of CaO/NH_2-MIL-101(Cr) composite.

2.2. Materials fabrication

2.2.1. Preparation of CaO nanoparticles from eggshells

Typically, 50 g of the gathered eggshells were cleaned with deionized water to get ride the pollutants and held for 2 h in a dry oven at 110 °C. The eggshells were then calcined at 1100 °C for 3 h in the muffle furnace. The solid produced was cooled, followed by stored in a desiccator (Fig. 1).

2.2.2. Fabrication of NH_2-MIL-101(Cr)

According to our previous work (Hassan et al., 2017; Aldawsari et al., 2020), the virgin NH_2-MIL-101(Cr) was produced by adding $Cr(NO_3)_3{\cdot}9H_2O$ (2 mmol, 800 mg), H_2N-BDC (2 mmol, 360 mg), and NaOH (5 mmol, 200 mg) to 30 mL DI water, agitating for 20 min. Then the blend was conveyed into a Teflon-lined autoclave reactor and held for 12 h at 150 °C. After centrifugation, the solid product was rinsed with DI water, ethanol, and dimethyl formamide (DMF), then dried under vacuum (Fig. 1).

2.2.3. In-situ preparation of CaO/NH_2-MIL-101(Cr) composite

The CaO with various dosage (Table 1) was firstly suspended in deionized water (15 mL) for 1 h and $Cr(NO_3)_3{\cdot}9H_2O$, H_2N-BDC and NaOH were transferred to the above suspen-

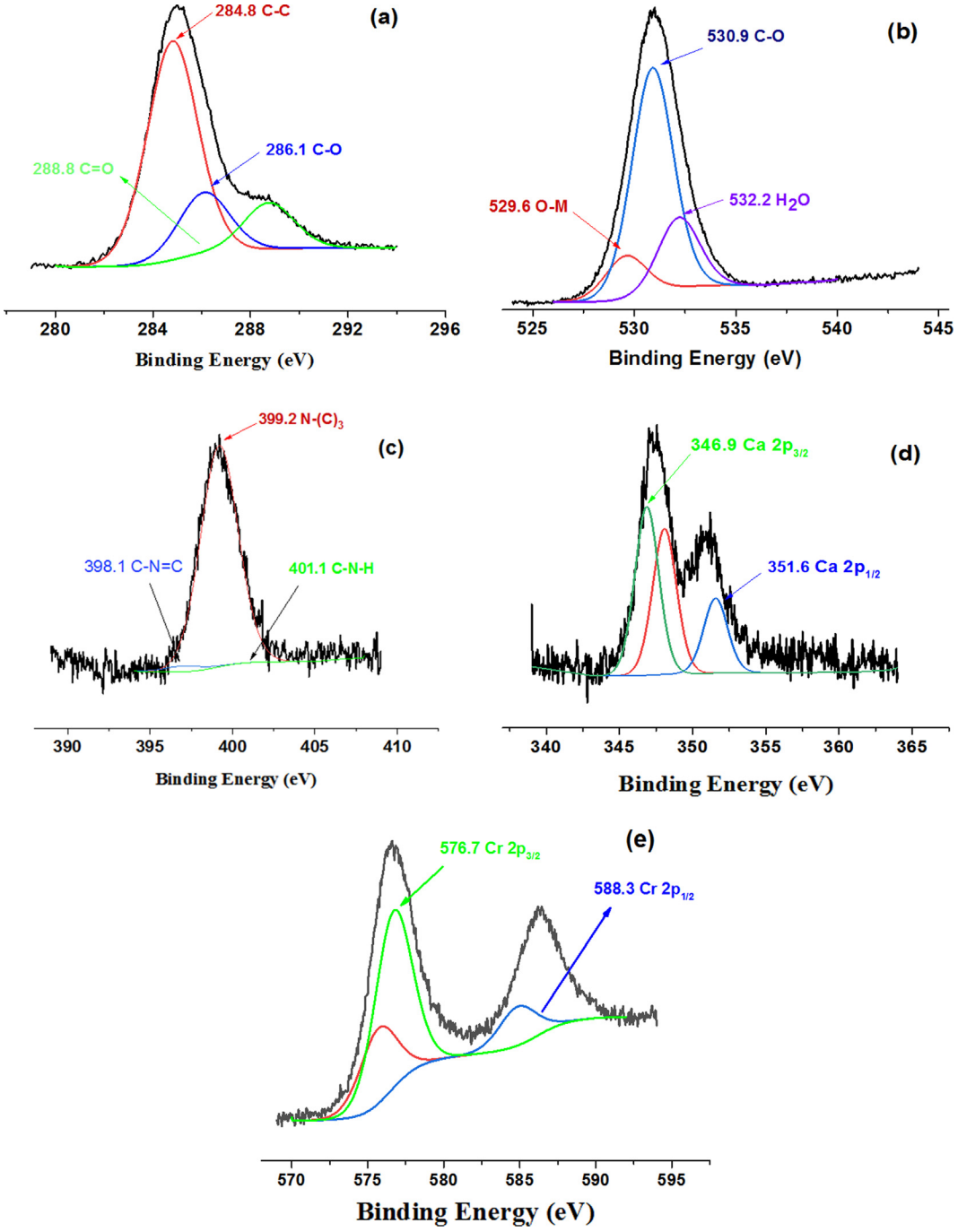

Fig. 3 XPS spectra of (0.04) CaO/NH_2-MIL-101(Cr) fashioned composite: C 1s (a), O 1 s (b), N 1 s (c), Ca 2p (d), and Cr 2p (e).

sion The blend was agitated for further 1 h and conveyed to a hydrothermal reactor, followed by heating in an oven at 150 °C for 12 h. The obtained product were then separated, rinsed with DI water, ethanol and dimethyl formamide (DMF), and dried under vacuum (Fig. 1).

2.3. Characterization

FT-IR spectra were obtained in the range of 4000–400 cm^{-1} using Shimadzu IR Tracer-100 (Shimadzu, 1 Nishinokyo Kuwabara-cho, Nakagyo-ku, Kyoto 604–8511, Japan). X-ray diffraction (XRD) were conducted using Cu-Kα radiation (1.54056 Å) at 40 kV and 40 mA by Shimadzu diffractometer (XRD7000). X-ray photoelectron spectroscopy (XPS) analysis on K-ALPHA (Thermo Fisher Scientific GmbH, Dreieich, Germany) was operated. The N_2 isotherms and surface characteristics was obtained at −196 °C using A NOVA 4200e (Quantachrome Instruments, Quantachrome GmbH & Co. KG, Boynton Beach, USA).

The Barrett–Joyner–Halenda (BJH) method was utilized to determine the pore size distributions employing the adsorption branch of the nitrogen isotherms. Thermogravimetric profiles (TGA) were performed on TGA-51 Shimadzu (25–600 °C, 10 °C min^{-1}, under flowing air gas). UV–vis spectra were measured on a UV Visible spectrophotometer Agilent Cary 60 Spectrophotometer (Agilent Technologies, USA). Scanning electron microscopy (SEM) images were gained with a Zeiss FESEM Ultra 60 and High-resolution transmission electron microscopy (HRTEM) images were collected via a JEOL-2011 electron microscope operated at 200 kV. The Knoevenagel reaction product of the catalytic reaction was followed by NMR-Jeol 600.

2.4. Basicity assessment

Acid titration of the basic centres offers a first sign of rising overall basicity as the CaO content increases. The quantitative assessment of the basic sites was performed by benzoic acid titration (Xie et al., 2006; Van Laar et al., 2001). For this experiment, the CaO/NH_2-MIL-101(Cr) composite (100 mg) was suspended with suitable volumes of toluene solution (3 mL, 0.1 mg/mL phenolphthalein (pKa = 9.3) indicator and maintained to equilibrium for 1 h. The solution was then titrated with (0.01 M) benzoic acid solution in toluene to assess the total basicity. Besides, the leached basicity was estimated by sonicating the composite aqueous solution (200 mg in 20 mL water) for 2 h at ambient temperature. Initially, the composite was collected by simple filtration, followed by the assessment of the solution pH followed by leachate titration with benzoic acid in methanol (0.01 M) using phenolphthalein.

2.5. Catalytic performance

The Knoevenagel condensation between benzaldehyde derivatives and an active methylene compound using CaO/NH_2-MIL-101(Cr) hybrid was performed in a magnetically stirred glass vial at 30 °C in THF. Typically, a blend of benzaldehyde (106 mg, 1.0 mmol) and malononitrile (100 mg, 1.5 mmol) was

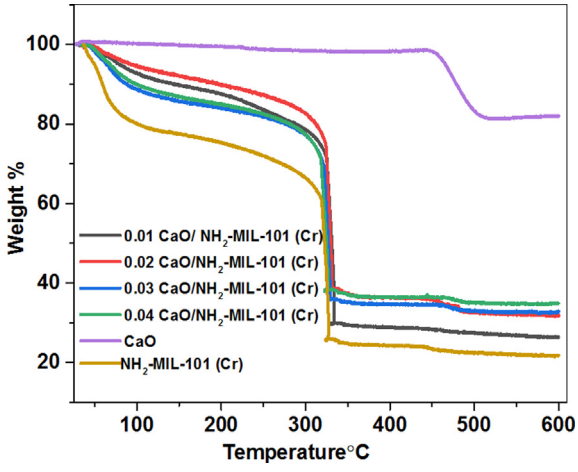

Fig. 4 TGA profiles of NH_2-MIL-101(Cr), CaO and fashioned composite CaO/NH_2-MIL-101(Cr) containing various dosage of CaO.

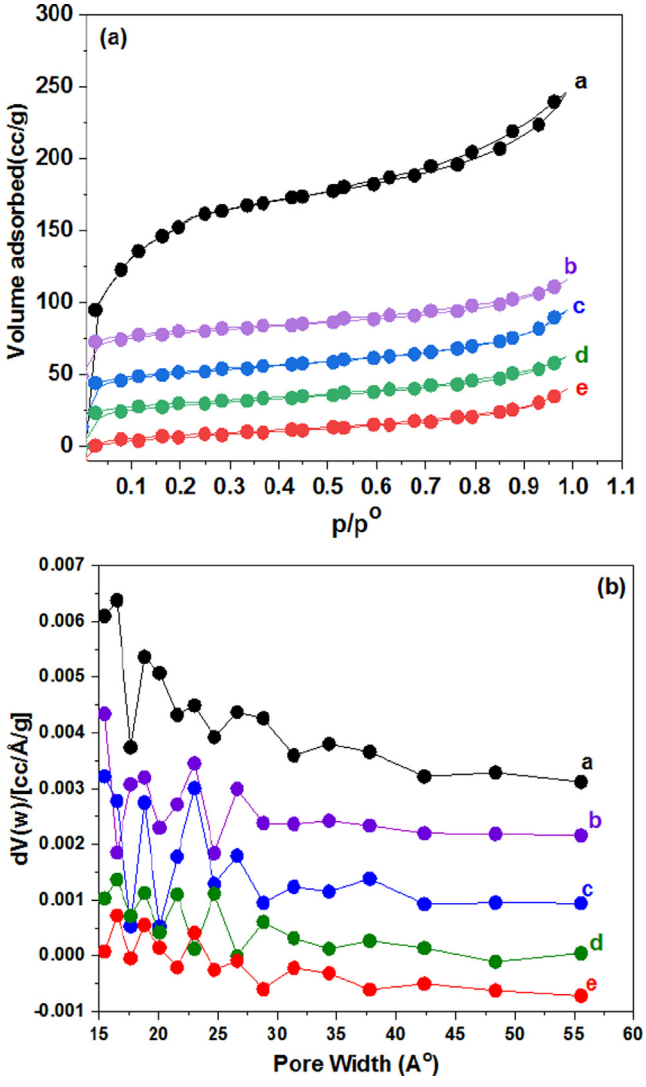

Fig. 5 (a) N_2 adsorption–desorption isotherms at −196 °C (b) pore size distribution of a: NH_2-MIL-101(Cr), b: (0.01) CaO/NH_2-MIL-101(Cr), c: (0.02) CaO/NH_2-MIL-101(Cr), d: (0.03) CaO/NH_2-MIL-101(Cr), and e: (0.04) CaO/NH_2-MIL-101(Cr).

dissolved in 10 mL of THF in a glass vial, and 1 mg of the CaO/NH_2-MIL-101(Cr) catalyst was introduced to it. The suspended blend solution was then stirred for 60 min. The catalyst was isolated from the reaction blend by centrifugation and under reduced pressure (30 mbar, 40 °C), the filtrate was then concentrated. The yield was calculated from ^{1}H NMR by comparing the magnitude of the integration signals of both unreacted aldehyde with the product. The (%) yield was evaluated for the reaction between 4-nitrobenzaldhyde and 2-(4-nitrobenzlidene) malononitrile, by compared the integral of the signal at δ 9.89 ppm (4-nitrobenzaldhyde) with those at δ 7.93 ppm (2-(4-nitrobenzlidene) malononitrile).

2.6. Catalyst recyclability

The reusability experiments were carried out to explore CaO/NH_2-MIL-101(Cr) stability in the Knoevenagel reaction by selecting the reaction between 4-nitrobenzaldyde with malononitrile as a model test reaction. The catalyst was also retrieved by centrifugation after each run from the reaction products and rinsed thoroughly with ethanol (~2 times, each time for ~ 60 min) and used for the subsequent measurment.

3. Results and discussion

3.1. Spectroscopic investigation

FT-IR spectra used to confirm the fabrication of the CaO/NH_2-MIL-101(Cr) composite. Fig. 2**a** illustrated the spectra of the CaO/NH_2-MIL-101(Cr) composite. The assigned bands at 1430 and 1620 cm^{-1} are related to the symmetrical and asymmetrical stretching vibrations of O-C-O respectively, suggesting the presence of di-carboxylic moieties (Ferreira et al., 2013). The characteristic bands in the range of 700–1300 cm^{-1}, are ascribed to the fingerprint vibration region of BDC (Petit and Bandosz, 2010). The absorption bands in the region of 760–861 cm^{-1} are related to the bending vibrations of C—H aromatic. The assigned bands of 1055 and 1150 cm^{-1} are related to C—N and C—O stretching modes, respectively. The peaks in between 400 and 700 cm^{-1} assigned to the featured Ca—O vibration was depicted for all the samples except NH_2-MIL-101(Cr) (Roy and Bhattacharya, 2011). Further, the intensity of absorption bands tends to be weaker with further increasing of CaO ratio.

To emphasize the NH_2-MIL-101(Cr) stability and confirm the fruitful synthesis of CaO/NH_2-MIL-101(Cr) composite, XRD was performed. The XRD patterns of the as-synthesized NH_2-MIL-101(Cr) and CaO/MIL-101(Cr) with various quantity of CaO loadings are displayed in Fig. 2**b**. The as-prepared NH_2-MIL-101(Cr) XRD pattern is quite similar to the simulated XRD pattern (**Figs. S1 in the Supporting Information**), with the distinctive diffraction peaks at 2θ = 2 .61°, 3.31°, 3.98°, 2.61°, 5.12°, 5.62°, 5.91°, 6.41°, 8.62°, 9.11°, 10.51°, 11.51° confirming the fruitful fabrication of NH_2-MIL-101(Cr) for eventual CaO NPs immobilizing. When comparing NH_2-MIL-101(Cr) and CaO/NH_2-MIL-101(Cr) to the simulated peak, the relative intensity changes for both. The presence of modest quantity of remain terephthalic acid and the insertion of CaO NPs into the MOF pores cause this behaviour (Hassan et al., 2017). The NH_2-MIL-101(Cr) displayed no obvious alteration in the crystal structure during the in-situ preparation of CaO/MIL-101(Cr) composite, indicating the great stability of the prepared MOF. The diffraction peaks from CaO NPs were not visible, which is mainly linked to lower CaO contents and the great dispersion of CaO within MOF pores. Also, NH_2-MIL-101(Cr) framework of is unchanged after use, as evidenced by similar XRD peaks before and after catalysis (Fig. 2**b**).

In order to further affirm the composite CaO/NH_2-MIL-101(Cr) fabrication and bonding, UV–vis absorption was recorded. The UV–vis spectra of the organic linker, NH_2-MIL-101(Cr) MOF and CaO/NH_2-MIL-101(Cr) are depicted in Fig. 2**c**. As shown in Fig. 2**c**, for the free organic linker, a strong characteristic band occurring at 345 nm may be attributed to transitions of π-π* and n-π*. In comparison, the NH_2-MIL-101(Cr) MOF and CaO/NH_2-MIL-101(Cr), absorption spectra deviated entirely from that of the free organic ligand, and a wide band of absorption was detected. Increased electron transfer between the Cr-oxo cluster and NH_2-BDC may have induced the broadening of the UV–vis spectra.This indicates that NH_2-BDC associate intensely with Cr-oxo clusters and participate in the fabrication of MOF and MOF composite.

^{1}H NMR were also performed to ensure the fruitful fabrication of the MOF and emphasize the structure stability after incorporation of CaO. ^{1}H NMR spectra of the NH_2-MIL-101 (Cr) MOF and (0.04) CaO/NH_2-MIL-101(Cr) were illustrated in Fig. 2**d**. It is clear that the chemical shift of the organic linker of the digested catalyst can be and the integral, which ver-

Table 2 Surface, texture and basicity characteristics for CaO/NH_2-MIL-101(Cr) composite nanoparticles containing various contents of CaO.

Catalysts	BET[a] (m^2g^{-1})	V_p[b] (cm^3g^{-1})	Total basicity (mmol/g)[c](mmol/g)	Leachable basicity (mmol/g)[d]	pH of H_2O suspension[e]
NH_2-MIL-101(Cr)	1032	0.34	0.31	–	3.8
CaO/NH_2-MIL-101(Cr)	801	0.26	0.65	0.03	7.2
CaO/NH_2-MIL-101(Cr)	638	0.23	0.87	0.04	7.4
CaO/NH_2-MIL-101(Cr)	588	0.22	1.12	0.08	7.9
CaO/NH_2-MIL-101(Cr)	290	0.13	1.34	0.11	8.1

[a] Surface area.
[b] Total pore volume.
[c] 0.1 g dried catalyst, suspended in 2 mL phenolphthalein solution (0.1 mg/mL), is titrated with (0.01 M) toluene solution of benzoic acid.
[d] Benzoic acid titration of the leachate in water in the presence of phenolphthalein as indicator.
[e] Suspension of 0.5 g catalyst in 100 mL deionized H_2O.

ified the fruitful modification, also matched. Evidently, the result offers strong proof on the successful fabrication of the composite and the MOF structure remained unchanged after the integration of CaO into MOF frameworks.

To estimate the real contents of CaO NPs loading on MOF surface, the ICP-AES was performed. The obtained results are tabulated in Table 1. The real CaO concentrations were found to be smaller than the stimulated values. The elemental compositions of (0.04) CaO/NH_2 -MIL-101(Cr) was assessed by XPS. The catalyst verified the existence of C, O, N, Ca, and Cr elements. The binding energy peaks at 284.8, 286.1, and 288.8 eV ascribed to C1s of C—C, C—O, and C═O, respectively (Fig. 3**a).** Binding energy peaks at 529.6, 530.9, and 532.2 eV in the O1s spectrum (Fig. 3**b**) could be assigned to C-O, O-M, and O-H, respectively. Other peaks located at 398.1, 399.2, and 401.1 eV related to C—N═C, N—$(C)_3$, and C—N—H (Fig. 3**c**). Also, as displayed in Fig. 3**d**, the bands of Ca cation are supported by the development of $2p_{3/2}$ and $2p_{1/2}$ at 347.6 and 352 eV, respectively that obviously displays the existence of CaO in the composite materials. Furthermore, Cr $2p_{3/2}$ and $2p_{1/2}$ have bands assigned to 576.7 eV and 588.3 eV, respectively, (Fig. 3**e**).

3.2. Thermal stability

The composite thermal stability was evaluated by the thermogravimetric experiments. The thermogravimetric profiles of NH_2-MIL-101(Cr), CaO, and CaO/NH_2-MIL-101(Cr) with various amount of CaO are displayed in Fig. 4. It worth noting that the TGA profile of CaO remained steady up to 454 °C. For NH_2-MIL-101(Cr), two weight-losses have been noted. The initial 18% weight loss happed at temperature less than 150 °C, which was related to the dehydration of physisorbed water, while the second weight-loss occurred at temperature around 320 °C which was linked to the framework degradation. The addition of CaO to NH_2-MIL-101(Cr) has a little effect on the thermal stability of the pure NH_2-MIL-101(Cr), as indicated by the slight increase in the degradation temperature from 320 to 325 °C in NH_2-MIL-101(Cr) and (0.04)CaO/NH_2-MIL-101(Cr) respectively.

3.3. Surface and textural properties

The N_2 adsorption–desorption measurements were performed to emphasize the porosity of viegin NH_2-MIL-101(Cr) and CaO/NH_2-MIL-101(Cr) composites. As depicted in Fig. 5**a**, All composites nanoparticles exhibited Type I isotherms which is a characteristics of materials which exhibited microporous nature (Sing et al., 1999). The pore size distribution of all fabricated composites are illustrated in Fig. 5**b,** which displays the existence of the similar pore size of 1.7 nm, suggesting the generation of micropores of MOF. Comparable isotherm shape was also realized in all materials, indicating that the overall NH_2-MIL-101(Cr) pores structure were unaffected after incorporation of CaO nanoparticles. The surface area of NH_2-MIL-101(Cr) attained 1032 m^2g^{-1}. The surface area of ((0.01) CaO/NH_2-MIL-101(Cr), (0.02) CaO/NH_2-MIL-101(Cr), (0.03) CaO/NH_2-MIL-101(Cr), and (0.04) CaO/NH_2-MIL-101(Cr)) composites were 801, 638, 588, and 290 m^2g^{-1} respectively, which were lesser than pure NH_2-MIL-101(Cr). Also, with increasing content of CaO up to 0.04 the total pore volume significantly decrease from 0.34 to 0.13 cm^3 g^{-1} (Table 2). This could be attributed to the incorporation of CaO, which had nearly a small surface area and CaO NPs occupying pores or blocking the outer surfaces of NH_2-MIL-101(Cr) with (Table 2). Therefore, it is speculated that the formed pore structure for the composite nanoparticles could be assigned to the blockage impact by CaO.

The morphology of (0.04) CaO/NH_2-MIL-101(Cr) with various were collected by FESEM as displayed in Fig. 6**(a &**

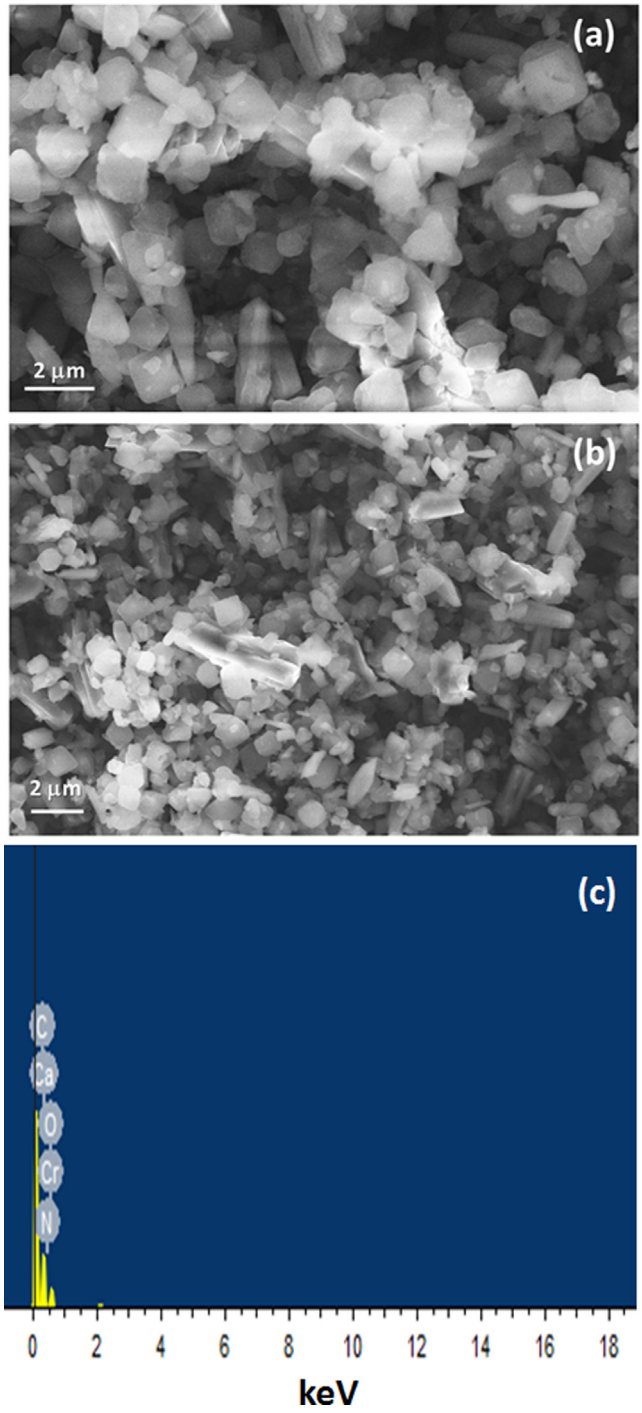

Fig. 6 **(a & b)** FESEM images and (c) EDS of the fashioned composite (0.04) CaO/NH_2-MIL- 101(Cr).

b). NH_2-MIL-101(Cr) exhibit an octahedron morphology with soft surface. Obviously, the morphology of the NH_2-MIL-101 (Cr) is appeared unchanged after incorporation of CaO which was in excellent agreement with XRD patterns. The element composition of the (0.04) CaO/NH_2-MIL-101(Cr) was obtained by EDS (Fig. 6**c**). The EDS assessment of the synthesized composite confirmed the bands attributed to C, O, N, Ca and Cr. The incorporation of CaO with NH_2-MIL- 101(Cr) were detected by HRTEM (Fig. 7**a & b)**). As can be shown, the crystal morphology of the MOF materials kept unchanged after immobilization of CaO species.The CaO NPs are clearly noted and uniformly dispersed throughout NH_2-MIL-101(Cr) with mean particle sizes of 4.4 nm for the sample containing CaO content of 0.04, which is considerably greater than the NH_2-MIL-101(Cr) pore size (1.7 nm) (Fig. 7**b**). As a result, the CaO nanoparticles covered multiple nearly pores in NH_2-MIL-101(Cr) instead of a single pore. The TEM images obtained significantly confirm the development of extremely dispersed CaO nanoparticles within the plentiful cavities of MIL-101(Cr)..

3.4. Basicity assessment

The color of an electrically neutral acid indicator immobilized from a toluene solution on the surface of a solid base is converted to its conjugate base, assuming the solid has the sufficient basic strength to give the acid electron pairs. The basic strength can therefore be evaluated by monitoring the indicators color changes over a range of values. In this work the basicity of the fashioned materials was monitored by various routes: (i) the pH measurement of the catalysts suspension in H_2O, (ii) the dried catalysts were blended with phenolphthalein (pKa = 9.3) in toluene solution, followed by a benzoic acid titration, and (iii) the leachable basicity was assessed by rinsed the catalysts (0.5 g) in water, followed by a benzoic acid titration of the leachate in the presence of phenolphthalein as indicator (Xie et al., 2006; Van Laar et al., 2001). Results are collected in Table 2. As can be shown, the existence of a pH indicator, like phenolphthalein, acid titration of the basic sites offers the first confirmation of increasing total basicity by increasing the CaO content in the hierarchical composite CaO/NH_2-MIL-101(Cr). The amount of the strong base sites (assessed using phenolphthalein as indicator) is gradually rising from (0.01) to (0.04) CaO. Furthermore, in accordance with the high calcium content, the composite containing (0.04) CaO displays both high leachable and total basicity. Finally, to assess the basicity characteristics of the hierarchical composite in completely hydrated environments, the suspensions pH comprising equal quantity of the composites with various CaO amount were determined. The pH rises from 3.8 for NH_2-MIL-101(Cr) to 8.1 for (0.04) CaO/NH_2-MIL-101 (Cr) composite. Based on all these findings, the composite with the greatest CaO content obviously offer the most basic environment and this could be mirrored in the catalytic performance of the Knoevenagel condensation.

3.5. Catalytic activity

Since the composite CaO/NH_2-MIL-101(Cr) provided both Lewis acidic, and basic sites at the same time, they may be applied as multipurpose catalysts. The Knoevenagel condensation of benzaldehyde with malononitrile was selected in this study as a model reaction using a set of CaO/NH_2-MIL-101 (Cr) composite comprising a various amount of CaO to assess the catalytic performance in a batch reaction (Scheme 1). Basic catalysts can facilely be activated the relatively acidic C-H bonds of malononitrile. We performed all our catalytic tests in tetrahydrofuran (THF) to eliminate any impact of the protic solvents that could be incredible for this kind of reaction as shown by Gascon et. al., (Gascon et al., 2009). The effect of different parameters such as CaO content, and substrate was addressed.

3.5.1. The influence of CaO content

For Knoevenagel condensation between 4-nitrobenzaldehyde and malonitrile, the catalytic perfoemance of CaO/NH_2-MIL-101(Cr) composite containing various content of CaO was assessed using 1 mg catalyst in THF at 30 °C for 60 min (Fig. 8). To further emphasize background rate and recognize the particular catalytic efficiency of the fabricated catalyst, multiple control tests were performed without the catalyst and under similar reaction conditions. Without a catalyst, the condensation reaction to generate the intended product is hard to initiate. At 30 °C for 60 min, a trace yield (less

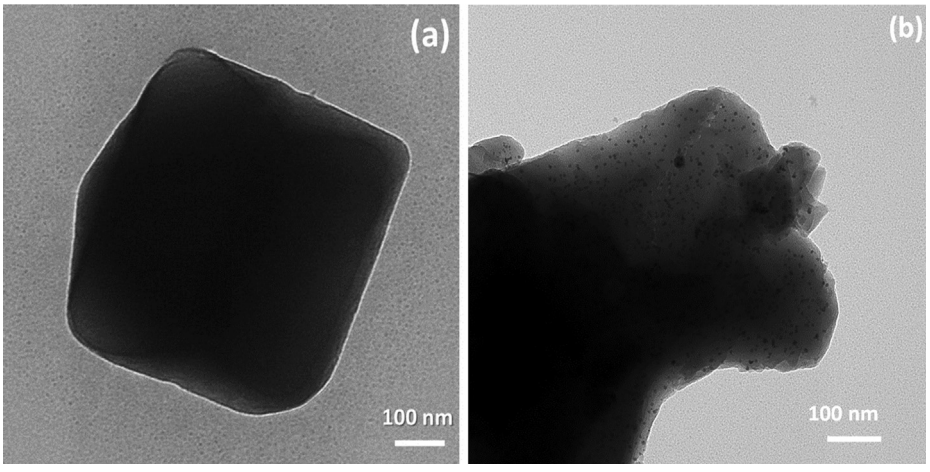

Fig. 7 HRTEM images (a) NH_2-MIL-101(Cr) and (b) the fashioned (0.04) CaO/NH_2-MIL-101(Cr) composite.

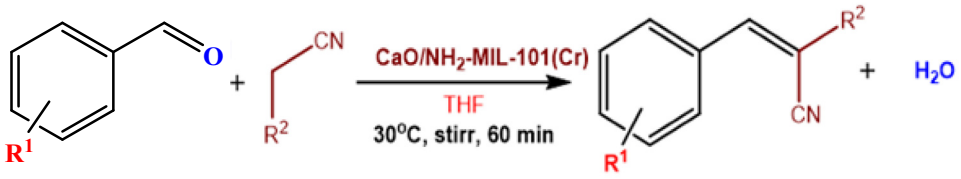

Scheme 1 Knoevenagel condensation.of benzaldehyde derivatives with malononitrile.

than2%) was noted. A little increase in the yield was obtained when pure NH_2-MIL-101(Cr) and CaO materials was added to catalyze the Knoevenagel condensation, suggesting that pure MOFs and CaO has shown poor performance (11%, and 20% respectively) under the similar reaction conditions. This behaviour may be due to the poor basic character of aromatic amine, with a Bordwell pK_a of 30.6 and a Bordwell pK_b of 4.87 (Bordwell, 1988). Due to the neighboring electron-withdrawing carboxylate moieties, the electrondensity of the amino group attached to benzene ring, along with its basicity, was decreased. Our approach is to immobilize a new species through in situ hydrothermal synthesis to improve the basic character of the heterogeneous MOF catalyst. The significantly enhanced basicity could make it possible to perform at a greater reaction rate with the Knoevenagel condensation reaction. As predicted, after 60 min reaction time, the novel CaO immobilized on NH_2-MIL-101(Cr) gave the desirable condensation product in 99% yield (Fig. 8). With increased CaO content, the catalytic efficiency vastly enhanced until the concentration reached (0.04) CaO. Furthermore, this result claimed that the catalytic performance relied heavily on the accessible immobilized CaO. Benzylidenemalonitrile was the reaction product derived from different catalysts, and no further by-products were reported. From the obtained findings, the immobilized CaO and NH_2-MIL-101(Cr) can be explained to have a synergistic action that is primarily assigned to the cohesion of the different basic sites. In particular, employing two routes for basic CaO/NH_2-MIL-101(Cr) composite, the catalytic process in Knoevenagel condensation can be addressed. One involves carboanion generation, oxy-anion formation, and water elimination imine intermediate mechanism (Han et al., 2014), and the other involves imine intermediate mechanism (Kubota et al., 2004; Chen et al., 2013). CaO/NH_2-MIL-101(Cr) with a combination acid-base site has a

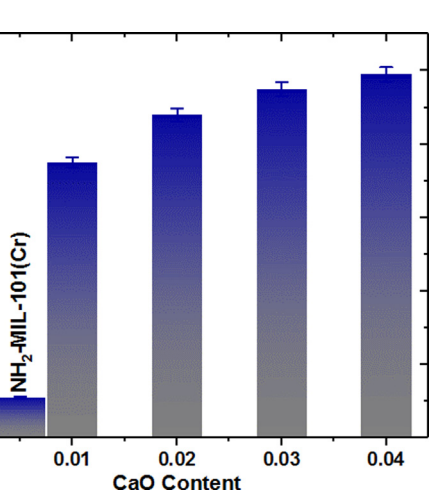

Fig. 8 Knoevenagel condensation of 4-nitrobenzaldehyde with malononitrile catalyzed by the composite. CaO/NH_2-MIL-101(Cr) containing various dosage of CaO.

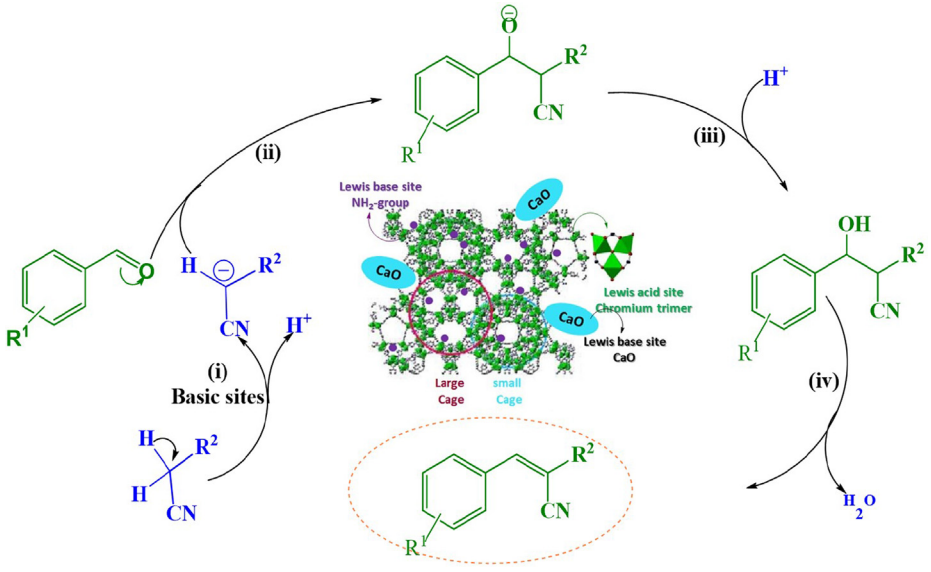

Scheme 2 Knoevenagel condensation reaction mechanism over CaO/NH_2-MIL-101(Cr) composite.

fantastic reaction boosting irrespective of the reaction mechanism. The immobilized CaO together with NH_2-MIL-101(Cr) as powerful fundamental sites help uptake the active methylene's proton of malononitrile to boost the generation of carboanion intermediate. Also, carbonyl moiety of benzaldehyde is polarized by the unsaturated Cr(VI) sites within the MOFs and a carbocation is developed. The carbanion attacks the carbocation, causing a dehydration process. As a result of the following, the products are created (Scheme 2). Consequently, the high CaO/NH_2-MIL-101(Cr) performance in Knoevenagel can be mainly explained to the synergistic phenomenon between CaO and NH_2-MIL-101(Cr).

3.5.2. Knoevenagel condensation using different substrates

As displayed in Table 3, the Knoevenagel condensation of different active methylene derivatives and different aldehydes were performed employing the acid-base bifunctional catalyst comprising (0.04) CaO/NH_2-MIL-101(Cr). It can be seen that, superior yields above 95% have been noted for most benzaldehyde derivatives comprising either electron withdrawing or donating moieties (**Entry 1–7**). In the Knoevenagel condensation reaction, nucleophilic addition is an obvious factor deciding the yield, so benzaldehyde dimethyl acetal derivatives comprising electron-withdrawing moities can render the process more convertible.

Table 3 Knoevenagel condensation results between benzaldehyde and malononitrile using (0.04) CaO/NH_2-MIL-101(Cr) composite

Entry	R^1	R^2	Product	Yield (%)[a]
1	H	CN	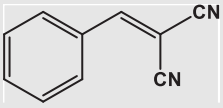	**96**
2	4-NO_2	CN	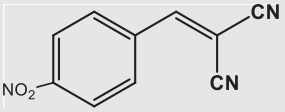	**99**
3	2-NO_2	CN	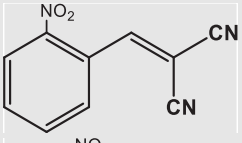	**98**
4	4-Cl	CN	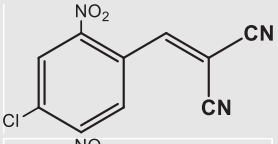	**98**
5	4-Br	CN	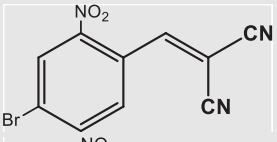	**96**
6	4-CN	CN	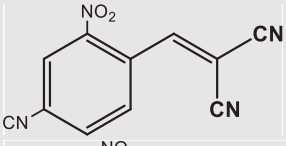	**99**
7	4-OCH_3	CN	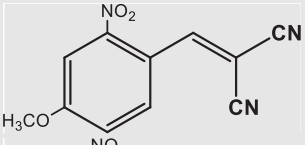	**96**
8	4-NO_2	$COOCH_3$	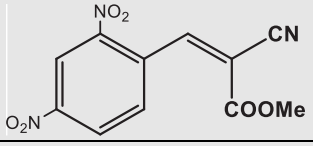	**90**

Reaction conditions: Aldehyde (1.0 mmol): Maloninitrile (1.5 mmol), (1 mg) catalyst, 60 min, 30 °C and THF.

[a] The yield was determined from the product's ^{1}H NMR analysis, calculating the integral product values and the unreacted aldehyde.

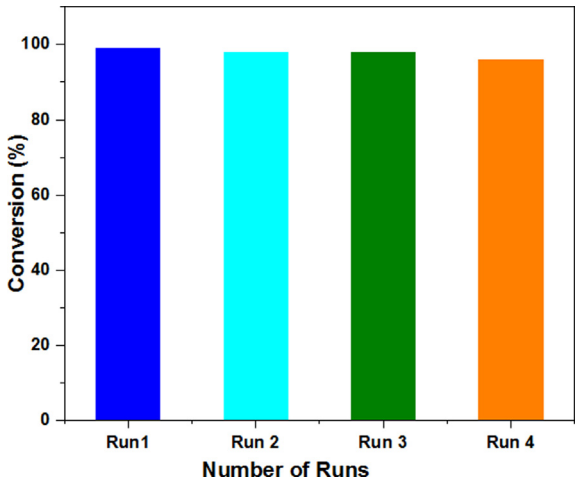

Fig. 9 Recycling performance of the fashioned composite (0.04) CaO/NH_2-MIL-101(Cr) in Knoevenagel condensation of 4-nitrobenzaldehyde with malononitrile.

In Knoevenagel condensation of 4-nitrobenzaldehyde with methylcyanoacetate under the given conditions in THF, the catalytic performance of the fabricated composite has also examined. It has been noted that the yields are not reduced significantly (90%) as shown in Table 3 (**Entry 8**). Thus, the substrate target of the prepared composite catalyzed Knoevenagel process is applicable for benzaldehyde components comprising withdrawing or donating moieties. Two key factors can be contributed to the excellent benchmark activity of our new composite catalyst; (i) NH_2-MIL-101(Cr) offer tailor-made pores and channels to boosting CaO dispersion and could also increase the mass transfer. (ii) The presence of acid-base synergistic steaming from multiple basic sites (CaO and NH_2–) and acidic site (chromium trimer) that promote the malononitrile deprotonating and nucleophilic attack, accordingly (see Scheme 2).

3.5.3. Proposed mechanism

In Scheme 2, a proposed Knoevenagel condensation mechanism of a carbonyl compound containing active methylene is presented. Basic sites (NH_2-groups and CaO) extract a proton from malononitrile's methylene carbon, resulting in a carbanion. Acidic Lewis sites (chromium trimer) activate the carbonyl of the aldehyde and a carbocation is formed. The carbanion that strikes the carbocation (ion dipole interaction) causes a dehydration reaction. The resulting removal of water helps in the producing of the final products (Benzylidene-malononitrile).

3.5.4. Catalyst reusability

Heterogeneous catalysts have the advantage of being easily recyclable and long-lasting. To show the catalyst durability, we selected the (0.04) CaO/NH_2-MIL-101(Cr) composite due to greater performance than the remaining MOFs composites that renders it more facile to handle. During the reaction, the fabricated composite is incredibly reliable and it could be reused at least four runs without losing its efficiency (Fig. 9).

4. Conclusion

In conclusion, a group of CaO immobilized NH_2-MIL-101(Cr), combining outstanding reusability were prepared by in-situ growth and scalable approach. The CaO NPs steadily boosted the surface basicity and the strength of the CaO/NH_2-MIL-101(Cr) catalysts up to (0.04) CaO loading. Due to the synergistic influence between the acidic and basic sites, the CaO/NH_2-MIL-101(Cr) composite demonstrate adequate catalytic efficiency in the Knoevenagel condensation. The catalyst containing (0.04) CaO displays the highest catalytic activity (conversion up to 99%). The performance were all greater than 90% under similar reaction conditions for benzaldehyde derivatives both withdrawing and donating electron moieties. The development of the non-precious metal oxide immobilized on MOFs nanoparticles intensified the employing of MOFs composite in the area of catalysis, and offered a viable strategy for the synthesis of multifunctional heterogeneous catalysts.

Declaration of Competing Interest

The authors declare that they have no known competing financial interests or personal relationships that could have appeared to influence the work reported in this paper.

Acknowledgment

The authors would like to thank the Deanship of graduate studies at Jouf University for funding and supporting this research through the initiative of DGS, Graduate Students Research Support (GSR) at Jouf University, Saudi Arabia. Additionally, the authors acknowledge the facilities operated by the central laboratory at Jouf University.

Appendix A. Supplementary material

Supplementary data to this article can be found online at https://doi.org/10.1016/j.arabjc.2021.103588.

References:

Cui, X., Li, W., Ryabchuk, P., Junge, K., Beller, M., 2018. Bridging homogeneous and heterogeneous catalysis by heterogeneous single-metal-site catalysts. Nat. Catal. 1, 385–397.

Matsunaga, S., Shibasaki, M., 2013. Multimetallic schiff base complexes as cooperative asymmetric catalysts. Synthesis (Stuttg) 45, 421–437.

Matsunaga, S., Shibasaki, M., 2014. Recent advances in cooperative bimetallic asymmetric catalysis: dinuclear Schiff base complexes. Chem. Commun. 50, 1044–1057.

Zhu, L., Liu, X.-Q., Jiang, H.-L., Sun, L.-B., 2017. Metal–organic frameworks for heterogeneous basic catalysis. Chem. Rev. 117, 8129–8176.

Xie, C., Yan, D., Li, H., Du, S., Chen, W., Wang, Y., Zou, Y., Chen, R., Wang, S., 2020. Defect Chemistry in Heterogeneous Catalysis: Recognition, Understanding, and Utilization. ACS Catal. 10, 11082–11098.

Yang, D., Gates, B.C., 2019. Catalysis by metal organic frameworks: perspective and suggestions for future research. ACS Catal. 9, 1779–1798.

Wang, P., Li, X., Zhang, P., Zhang, X., Shen, Y., Zheng, B., Wu, J., Li, S., Fu, Y., Zhang, W., 2020. Transitional MOFs: Exposing Metal Sites with Porosity for Enhancing Catalytic Reaction Performance. ACS Appl. Mater. Interfaces 12, 23968–23975.

Cheng, P., Wang, C., Kaneti, Y.V., Eguchi, M., Lin, J., Yamauchi, Y., Na, J., 2020. Practical MOF nanoarchitectonics: new strategies for enhancing the processability of MOFs for practical applications. Langmuir 36, 4231–4249.

Tran, U.P.N., Le, K.K.A., Phan, N.T.S., 2011. Expanding applications of metal– organic frameworks: zeolite imidazolate framework ZIF-8 as an efficient heterogeneous catalyst for the knoevenagel reaction. Acs Catal. 1, 120–127.

Abd El Rahman, S.K., Hassan, H.M.A., El-Shall, M.S., 2014. Metal-organic frameworks with high tungstophosphoric acid loading as heterogeneous acid catalysts. Appl. Catal. A Gen. 487, 110–118.

Hassan, H.M.A., Betiha, M.A., Mohamed, S.K., El-Sharkawy, E.A., Ahmed, E.A., 2017. Stable and recyclable MIL-101 (Cr)–Ionic liquid based hybrid nanomaterials as heterogeneous catalyst. J. Mol. Liq. 236, 385–394.

El-Shall, M.S., Abdelsayed, V., Abd El Rahman, S.K., Hassan, H.M. A., El-Kaderi, H.M., Reich, T.E., 2009. Metallic and bimetallic nanocatalysts incorporated into highly porous coordination polymer MIL-101. J. Mater. Chem. 19, 7625–7631.

Alhumaimess, M.S., Alsohaimi, I.H., Hassan, H.M.A., El-Sayed, M. Y., Alshammari, M.S., Aldosari, O.F., Alshammari, H.M., Kamel, M.M., 2020. Synthesis of ionic liquid intercalated layered double hydroxides of magnesium and aluminum: A greener catalyst of Knoevenagel condensation. J. Saudi Chem. Soc. 24, 321–333.

Wee, L.H., Janssens, N., Sree, S.P., Wiktor, C., Gobechiya, E., Fischer, R.A., Kirschhock, C.E.A., Martens, J.A., 2014. Local transformation of ZIF-8 powders and coatings into ZnO nanorods for photocatalytic application. Nanoscale. 6, 2056–2060.

Liu, Q., Low, Z.-X., Li, L., Razmjou, A., Wang, K., Yao, J., Wang, H., 2013. ZIF-8/Zn_2GeO_4 nanorods with an enhanced CO_2 adsorption property in an aqueous medium for photocatalytic synthesis of liquid fuel. J. Mater. Chem. A. 1, 11563–11569.

Zhang, T., Zhang, X., Yan, X., Kong, L., Zhang, G., Liu, H., Qiu, J., Yeung, K.L., 2013. Synthesis of Fe_3O_4@ZIF-8 magnetic core–shell microspheres and their potential application in a capillary microreactor. Chem. Eng. J. 228, 398–404.

Wang, W., Li, Y., Zhang, R., He, D., Liu, H., Liao, S., 2011. Metal-organic framework as a host for synthesis of nanoscale Co_3O_4 as an active catalyst for CO oxidation. Catal. Commun. 12, 875–879.

Li, Z., Wang, C., Chen, X., Wang, X., Li, X., Yamauchi, Y., Zhao, X. S., 2020. MoOx nanoparticles anchored on N-doped porous carbon as Li-ion battery electrode. Chem. Eng. J. 381, (2020) 122588.

Li, X., Lin, B., Li, H., Yu, Q., Ge, Y., Jin, X., Xiao, J., 2018. Carbon doped hexagonal BN as a highly efficient metal-free base catalyst for Knoevenagel condensation reaction. Appl. Catalysis B: Environ. 239, 254–259.

Parida, K.M., Rath, D., 2009. Amine functionalized MCM-41: An active and reusable catalyst for Knoevenagel condensation reaction. J. Mol. Catal. A Chem. 310, 93–100.

Zhao, S., Wang, X., Zhang, L., 2013. Rapid and efficient Knoevenagel condensation catalyzed by a novel protic ionic liquid under ultrasonic irradiation. RSC Adv. 3, 11691–11696.

Villa, A., Tessonnier, J.-P., Majoulet, O., Su, D.S., Schlögl, R., 2010. Transesterification of triglycerides using nitrogen-functionalized carbon nanotubes. ChemSusChem 3, 241.

Mondal, J., Modak, A., Bhaumik, A., 2011. Highly efficient mesoporous base catalyzed Knoevenagel condensation of different aromatic aldehydes with malononitrile and subsequent noncatalytic Diels-Alder reactions. J. Mol. Catal. A Chem. 335, 236–241.

Aromi, G., Barrios, I.A., Roubeau, O., Gamez, P., 2011. Coord. Chem. Rev. 255, 485–546.

Hasegawa, S., Horike, S., Matsuda, R., Furukawa, S., Mochizuki, K., Kinoshita, Y., Kitagawa, S., 2007. Three-dimensional porous coordination polymer functionalized with amide groups based on tridentate ligand: selective sorption and catalysis. J. Am. Chem. Soc. 129, 2607–2614.

Stewart, R., Dolman, D., 1967. A comparison of the acidity and basicity of aromatic amines. Can. J. Chem. 45, 925–928.

Zhang, J.-P., Zhang, Y.-B., Lin, J.-B., Chen, X.-M., 2012. Metal azolate frameworks: from crystal engineering to functional materials. Chem. Rev. 112, 1001–1033.

Hwang, Y.K., Hong, D., Chang, J., Jhung, S.H., Seo, Y., Kim, J., Vimont, A., Daturi, M., Serre, C., Férey, G., 2008. Amine grafting on coordinatively unsaturated metal centers of MOFs: consequences for catalysis and metal encapsulation. Angew Chemie 120, 4212–4216.

Li, B., Zhang, Y., Ma, D., Li, L., Li, G., Li, G., Shi, Z., Feng, S., 2012. A strategy toward constructing a bifunctionalized MOF catalyst: post-synthetic modification of MOFs on organic ligands and coordinatively unsaturated metal sites. Chem. Commun. 48, 6151–6153.

Chen, J., Liu, R., Gao, H., Chen, L., Ye, D., 2014. Amine-functionalized metal-organic frameworks for the transesterification of triglycerides. J. Mater. Chem. A. 2, 7205–7213.

Trilla, M., Pleixats, R., Man, M.W.C., Bied, C., 2009. Organic–inorganic hybrid silica materials containing imidazolium and dihydroimidazolium salts as recyclable organocatalysts for Knoevenagel condensations. Green Chem. 11, 1815–1820.

Hassan, H.M.A., Betiha, M.A., Mohamed, S.K., El-Sharkawy, E.A., Ahmed, E.A., 2017. Salen-Zr (IV) complex grafted into amine-tagged MIL-101 (Cr) as a robust multifunctional catalyst for biodiesel production and organic transformation reactions. Appl. Surf. Sci. 412, 394–404.

Aldawsari, A.M., Alsohaimi, I.H., Hassan, H.M.A., Berber, M.R., Abdalla, Z.E.A., Hassan, I., Saleh, E.A.M., Hameed, B.H., 2020. Activated carbon/MOFs composite: AC/NH2-MIL-101 (Cr), synthesis and application in high performance adsorption of p-nitrophenol. J. Saudi Chem. Soc. 24, 693–703.

Xie, W., Peng, H., Chen, L., 2006. Calcined Mg–Al hydrotalcites as solid base catalysts for methanolysis of soybean oil. J. Mol. Catal. A Chem. 246, 24–32.

Van Laar, F., De Vos, D.E., Pierard, F., Kirsch-De Mesmaeker, A., Fiermans, L., Jacobs, P.A., 2001. Generation of singlet molecular oxygen from H2O2 with molybdate-exchanged layered double hydroxides: effects of catalyst composition and reaction conditions. J. Catal. 197, 139–150.

Ferreira, R.B., Scheetz, P.M., Formiga, A.L.B., 2013. Synthesis of amine-tagged metal–organic frameworks isostructural to MIL-101 (Cr). RSC Adv. 3, 10181–10184.

Petit, C., Bandosz, T.J., 2010. Enhanced adsorption of ammonia on metal-organic framework/graphite oxide composites: analysis of surface interactions. Adv. Funct. Mater. 20, 111–118.

Roy, A., Bhattacharya, J., 2011. Microwave assisted synthesis of CaO nanoparticles and use in waste water treatment. Nano Technol. 3, 565–568.

Sing, K.S.W., Rouquerol, F., Rouquerol, J., 1999. Adsorption By Powders and Porous Solids: Principles, Methodology, and Applications. Academic Press.

Gascon, J., Aktay, U., Hernandez-Alonso, M.D., van Klink, G.P.M., Kapteijn, F., 2009. Amino-based metal-organic frameworks as stable, highly active basic catalysts. J. Catal. 261, 75–87.

Bordwell, F.G., 1988. Equilibrium acidities in dimethyl sulfoxide solution. Acc. Chem. Res. 21, 456–463.

Han, J., Xu, G., Ding, B., Pan, J., Dou, H., MacFarlane, D.R., 2014. Porous nitrogen-doped hollow carbon spheres derived from polyaniline for high performance supercapacitors. J. Mater. Chem. A. 2, 5352–5357.

Kubota, Y., Nishizaki, Y., Ikeya, H., Saeki, M., Hida, T., Kawazu, S., Yoshida, M., Fujii, H., Sugi, Y., 2004. Organic–silicate hybrid catalysts based on various defined structures for Knoevenagel condensation. Microporous Mesoporous Mater. 70, 135–149.

Chen, X., Arruebo, M., Yeung, K.L., 2013. Flow-synthesis of mesoporous silicas and their use in the preparation of magnetic catalysts for Knoevenagel condensation reactions. Catal. Today. 204, 140–147.